ICAS-80-7.2 INVESTIGATION OF HIGH-MANOEUVRABILITY FLIGHT VEHICLE DYNAMICS

Martin E. Beyers†
Council for Scientific and Industrial Research
Pretoria, South Africa.

Abstract

The potential role of wind tunnel free-flight experiments in the flight dynamic analysis of high-performance aircraft and missiles is examined. The usefulness of the approach is seen to be not only contingent on the ability to extract aerodynamic derivatives, but also lies in the broader objective of aerodynamic data/mathematical model validation. Experimental and analytical techniques were developed to study the generic nonoscillatory motion of high-manoeuvrability vehicles in free flight and subsequently investigated in depth. The stability derivatives of a destabilized, air-to-air missile configuration were determined in free flight at Mach 0,7, revealing highly nonlinear behaviour and, in particular, a discontinuous dynamic stability characteristic at medium angles of attack. The feasibility of aircraft model free-flight tests is demonstrated on the basis of simulations and a trajectory validation scheme proposed for the corroboration of free-flight and captive-model dynamic data.

Introduction

The continued demands of increased manoeuvrability in high-performance aircraft and missiles have led to a deepening emphasis on flight at high angles of attack and high rotation rates and concomitantly revealed the complexity of the associated nonlinear flight dynamic characteristics. The incomplete success of many flight predictions under these conditions, based on available wind tunnel data, may be largely attributable to inadequacies of the mathematical models used and to the difficulties associated with interpretation of experimental dynamic stability data.

This paper is concerned with recent developments in the field of free-flight testing which have made it possible to evaluate, under realistic motion conditions, some of the dynamic parameters required to predict the behaviour of high-manoeuvrability flight vehicles, and to achieve validation of the aerodynamic force model and dynamic data used in the simulation of such behaviour.

Previously, the wind tunnel free-flight technique had been restricted to statically stable models of symmetrical re-entry vehicles[1,2] and missile configurations[3,4] in ballistic flights at near-zero trim angles. The successful implementation of the new experimental and analytical concepts in the study of the free motion of a missile trimmed at significant angles of attack marked a distinct augmentation of the basic free-flight capability, which has brought the possibility of similar tests on fighter aircraft models within reach.

In contrast to stable ballistic motion which is characterized by angular oscillations about a mean position, the responses of statically unstable or bistable configurations are essentially *nonoscillatory*. Therefore, whereas oscillatory model tests are required to study the former, the investigation of marginally-stable uncontrolled motion, like controlled motion, requires a small-amplitude, large-angle experimental analogue. Such angular motion conditions can be obtained in either captive-model forced oscillation or nonoscillatory free-flight experiments.

The techniques for nonoscillatory free-flight experiments were introduced in a series of papers[5-10] and subsequently described in detail[11,12]. The pitch-jet model launching system[8] overcomes difficulties previously experienced in flying lifting models by imparting optimal initial conditions at launching. Moreover, since available data reduction procedures were quite inadequate for the analysis of nonoscillatory motion, a new approach of reducing the angular motion by means of a reconstruction procedure in conjunction with a local aerodynamic analysis (RL) technique was introduced[5,7,11]

The first example of vehicles in the high-manoeuvrability category to be studied by means of this approach was a hypothetical air-to-air missile[8,9]. A summary of the experimental programme[9,11] is presented in this paper. Subsequently, the approach was generalized to be applicable to other vehicles in the category[11]. The extension to aircraft model tests at angles of attack up to 40° is investigated on the basis of simulated 6 DOF wind tunnel trajectories and possible methods for the extraction of direct and cross-coupling derivatives are considered. Aircraft dynamic cross-coupling derivatives were first isolated by Orlik-Rückemann, et al[13-15] and Hanff, et al[16], in captive model tests of an aircraft-like configuration. A method is proposed here for the indirect corroboration of these data with free-flight results on the same model.

Dynamic Testing Rationale

As a result of the highly nonlinear nature of vehicle dynamics in manoeuvring flight where the air flows are governed by asymmetric, hysteretic flow mechanisms, such flight is fundamentally a six-

†Head, Flight Mechanics Division,
National Institute for Aeronautics and Systems Technology.
Member AIAA

degree-of-freedom (6 DOF) phenomenon which currently cannot be approached theoretically. An analysis based on experimental data would be complete only if (a) comprehensive dynamic characteristics could be determined under conditions of free motion representative of full-scale flight, or if (b) the dynamic derivatives obtained for simple, one-degree-of-freedom motions are free of uncertainty due to support interference, and can be correctly synthesized in a mathematical model which accounts for the motion shape and time-history dependencies which might exist. Unfortunately, neither of these two ideals have been realized and the most logical expedient is the best possible compromise between (a) and (b), utilizing the partial solutions afforded by existing techniques. The nature of the compromise will necessarily be dictated by individual needs and capabilities, but to have a chance of success in the absence of complete understanding of the aerodynamic phenomena involved, the analysis of a flight vehicle cannot be complete without appropriate free-motion studies.

A comprehensive mathematical model is also prerequisite to flight dynamic analysis and, in particular, to the development of aircraft having good flying qualities at high angles of attack. An essential ingredient of the aircraft mathematical model is an aerodynamic force model which formulates the forces and moments acting on the vehicle at the flight conditions under consideration. The force model may be expressed in terms of expansions of the aerodynamic derivatives about a steady state condition where the nature and number of the coefficients are dictated, in part, by the availability of dynamic stability data. For fixed control surfaces, this could take the form

$$C_i = C_{i_o} + C_{i_{(\alpha,\beta,\nu)}} + C_{i_{\zeta_j}}(\alpha,\beta,\bar{\zeta}_j)\frac{\zeta_j d}{2V} + C_{i_{\omega_k}}(\alpha,\beta,\bar{\omega}_k)\frac{\omega_k d}{2V}, \quad (1)$$

where C_i ($i = Y,Z,\ell,m,n$) are the aerodynamic coefficients, α and β are the angles of attack and sideslip, and ζ_j, ω_k and ν ($\zeta_j = \dot{\alpha}, \dot{\beta}$; $\omega_k = p,q,r$) are respectively the generalized accelerations, frequencies and the coning rate, d is the reference length and V the velocity.

Because of the complexity of the aircraft mathematical model, including aerodynamics, propulsion and control systems and airframe dynamics, the formulations of these subsystems must be verified independently. Aircraft scale models can provide overall validation of gross flight dynamic effects as represented by the mathematical model (as in spin testing). Controlled free-flight tests in wind tunnels, on the other hand, provide the means for verifying the aerodynamic force model independently as well as for studying its individual features in isolation. The latter objective necessitates adequate control over motion conditions so that the number of effective variables can be reduced, without sacrificing the representativeness of the motion simulated. This may be thought of as an extension of the role played by captive dynamic tests, *viz.*, studying individual simplified motions in isolation, where the mechanical constraints are removed here. Simulation results may conceivably be more realistic when based on derivatives extracted from free-flight rather than captive model tests, by virtue of, *inter alia*, the tendency for possible force model inadequacies to be fortuitously accounted for in the former case. For instance, the effects of higher-order derivatives omitted from Eq. (1) (such as those due to $\dot{p}$ or $\dot{q}$) will be lumped together with their first-order counterparts in the pertinent planes and have the correct magnitudes, provided that the simulated motions resemble those reduced for the derivatives and that the same force model is used in both cases.

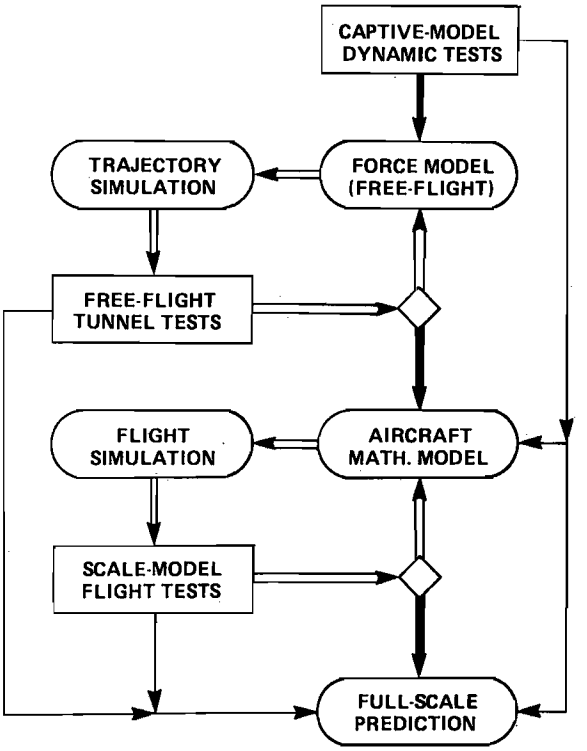

Fig. 1 Mathematical model validation scheme

A realistic scheme for the validation of the force model and the overall mathematical model is illustrated in Figure 1. Inputs from captive as well as free-flight dynamic stability experiments are fed to a computer simulation incorporating the force model, which may then be improved by systematic adjustments to match the model-scale wind tunnel flight. Subsequently, the overall mathematical model may be validated in a similar fashion by correlation with scale model flight test results, and finally, applied to full-scale flight after extrapolating the dynamic data to full-scale Reynolds numbers.

It may, of course, be impossible to simulate directly full-scale dynamic behaviour at subscale Reynolds numbers[17]; hence the need for analytical extrapolation of the dynamic data obtained in both captive and free-flight tests. It is well known that additonal problems complicate the interpretation of captive dynamic test data, namely, support interference[18] and motion constraints[11,19]. The credibility of these data could be enhanced through the force model validation scheme described; if

quantitative correlation can be achieved in this way between the data obtained from the two methods, the force model as well as the accuracy of the captive dynamic data would at once be established.

Free-flight tests can therefore provide the complete laboratory analogue of the uncontrolled flight of a high-performance aircraft which, while difficult to analyze independently, potentially fulfils an important role in the overall flight dynamics prediction:Even when the free-flight Reynolds numbers are quite unrealistic, the experiment is nevertheless a powerful tool in the validation of the aircraft force model.

Analysis

The nature of the problem of nonoscillatory free-flight motion is illustrated by the example of a simulated wind-tunnel flight of a destabilized missile model. The pitch angle is plotted as a function of time t in Figure 2, revealing a slight "kink" near 0,04 s, before settling down to a trim angle of -5°. If the initial amplitude θ_o should be reduced from 22° to say 20°, the curve will turn upwards at this point (due to insufficient angular momentum) and fall into a positive trim angle of +5°. There is thus a minimum value of θ_o for the observation of a half-cycle terminal oscillation which is accompanied by a minimum swerve displacement. Once the trim point is reached, the lateral displacement rapidly grows beyond the limits of observation in the test section. The situation arises as a result of the high damping and instability at small angles, and is further complicated by the effects of induced rolling moments.

Similarly, in a large-amplitude motion, there is a minimum value of θ_o for one-cycle terminal oscillatory motion, and while the analogy might be extended to $1\frac{1}{2}$ cycles it is found, in practice, that after the first two peaks (*i.e.* one cycle) the lateral displacement will invariably diverge beyond the observation limit. From this it follows that, unless the model size is reduced, the high angle-of-attack- and trimming motions have to be studied separately. Both the half- and one-cycle terminal motions are denoted *nonoscillatory* since, by their very nature, the truncated oscillations cannot be sustained.

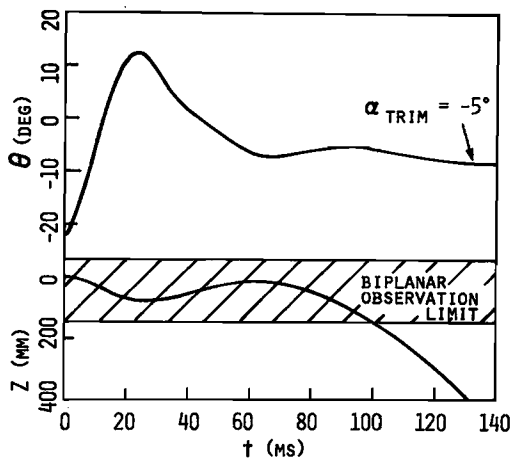

Fig. 2 Simulated flight of a bistable model

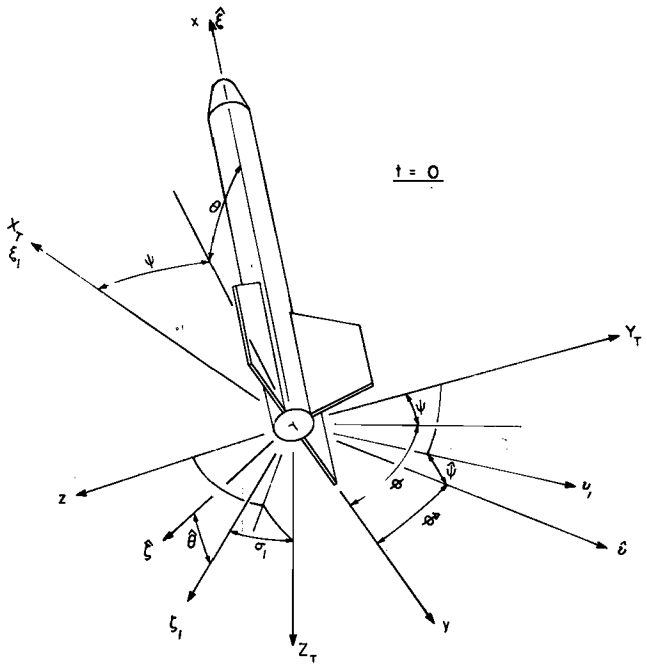

Fig. 3 Reference systems for data reduction

The standard data reduction techniques applicable to oscillatory motion are clearly not suited to the analysis of such flights. A detailed exposé of the methods developed for this purpose was published elsewhere[11] and only the salient aspects can be summarized in this paper.

Data Transformation

The minimal angular responses of nonoscillatory free flight impose most stringent accuracy criteria on data acquisition and reduction systems alike. Accordingly, a sophisticated biplanar optical data acquisition system was developed and very complete data transformation equations were derived, whereby all significant sources of error could be accounted for and effectively eliminated.

Frames of reference for data reduction are depicted in Figure 3, including the horizontal tunnel system (X_T, Y_T, Z_T) and one of the biplanar axes systems (ξ_1,υ_1,ζ_1), the body axes system (x, y,z) and an inclined fixed-plane system ($\hat{\xi},\hat{\upsilon},\hat{\zeta}$). ψ,θ,ϕ and $\hat{\psi},\hat{\theta},\hat{\phi}$ are respectively the modified Euler angles in the horizontal and inclined systems. The relationship between displacements Y_T,Z_T, and ζ_1,ζ_2 may be derived from Figure 4:

$$Y_T = (\zeta_2 \cos \sigma_1 - \zeta_1 \cos \sigma_2)/\sin(\sigma_2 - \sigma_1)$$
$$Z_T = (\zeta_2 \sin \sigma_1 - \zeta_1 \sin \sigma_2)/\sin(\sigma_1 - \sigma_2) \qquad (2)$$

where σ_1 and σ_2 are the top and bottom viewing angles respectively. The biplanar angle transformation follows directly from Eq. (2) since the projected angles are geometrically related to their linear counterparts (e.g.ζ_i = tan θ_i).

Figure 5 illustrates physical quantities in the inclined system. Here OP is the wing or tail trailing edge, s is the wingspan and s_1 its projection, s_a is the apparent or measured span and ψ_1, θ_1,ϕ_1 are the projected position angles. For

convenience, the complement of the roll angle $\hat{\phi}^*$ is shown. The oblique projection of $\hat{\phi}$ is

$$\phi_p = \cos^{-1}(s_1/s) \qquad (0 < \phi_a \leq \pi/4)$$
$$\phi_p = \pi/2 - \cos^{-1}(s_1/s) \quad (\pi/4 < \phi_a < \pi/2) \tag{3}$$

where the projection of the trailing edge is $s_1 = s_a/\sin(\theta_{TE} + \theta_1)$ and $\phi_a = \cos^{-1}(s_a/s)$. The implicit ambiguity is resolved by an independent measurement to determine the direction of rotation. Then the Euler angle of roll is given by

$$\phi = \text{sign}(p)\{n - (\text{sign}(p)(1) - 1)/2\}\pi/2 + \phi_+ \tag{4}$$

where n is an integer and

$$\phi_+ = \tan^{-1}\{(\tan\phi_y \cos\theta + \sin\psi \sin\theta)/\cos\psi\} \tag{5}$$

$$\phi_y = \tan^{-1}\{\tan\phi_p/\sin\theta_{TE}\} - \sigma_1 \tag{6}$$

In principle, it is possible to obtain all three Euler angles from the information contained in a single plane. Using the relationship

$$\cos\phi^* = (s^2 - s_1^2 + s_1 OA \tan\psi \cos\theta_{TE})/(s.OB) \tag{7}$$

and Eq. (3), the following expression may be derived

$$\phi_+ = \sin^{-1}\{\cos\psi \sin\phi_p + \sin\psi \cos\phi_p \cos\theta_{TE}\} \tag{8}$$

θ is directly measurable, and if ϕ can be measured independently, then Eq. (8) may be solved for the yaw angle ψ.

The motion of the missile centre of mass is referred to the "flight coordinate system" (X,Y,Z) which is parallel to the inertial tunnel frame of reference (X_T,Y_T,Z_T) and moves along X_T at a velocity V_∞. The free-flight data are transformed to the aeroballistic and aerodynamic frames of reference $(\hat{x},\hat{y},\hat{z})$ and $(\acute{x},\acute{y},\acute{z})$. The aeroballistic system is a body-fixed frame inclined relative to (X,Y,Z) through the angles due to swerve,

$$\gamma_y = \tan^{-1}\frac{dy}{dx}, \quad \gamma_z = \tan^{-1}\frac{dz}{dx} \tag{9}$$

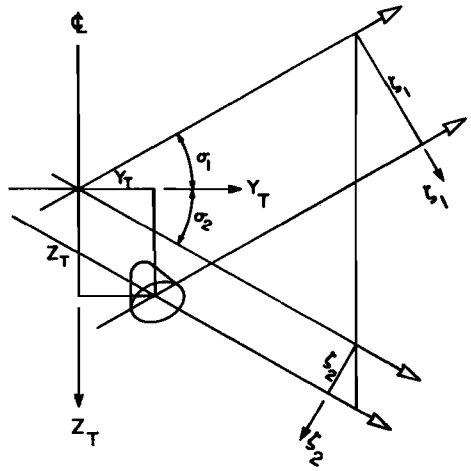

Fig. 4 Lateral displacements

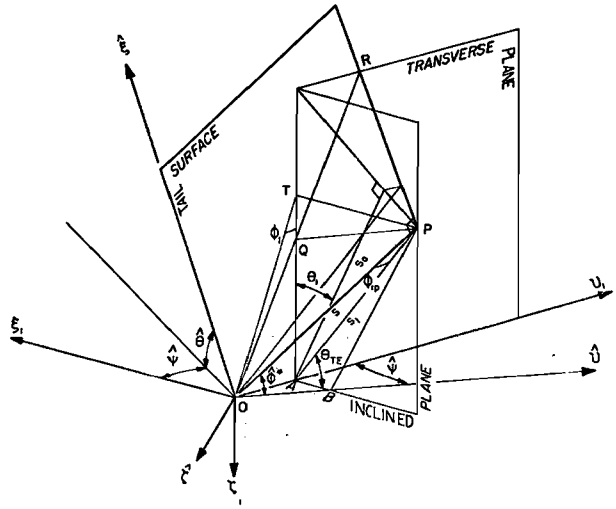

Fig. 5 Tail surface in the inclined system

Then, using the missile convention

$$\hat{\beta} = \sin^{-1}\frac{\hat{v}}{V}, \quad \hat{\alpha} = \sin^{-1}\frac{\hat{w}}{V} \tag{10}$$

where $\hat{u},\hat{v},\hat{w}$ are the body axes velocities, the general expressions for the aeroballistic angles of attack and sideslip in terms of the projected angles were obtained as follows

$$\sin\hat{\beta} = \sin\{(-\psi + \gamma_y)\cos\gamma_z\}$$
$$\sin\hat{\alpha} = \sin\{\tan^{-1}(\tan\theta_z \cos\psi) + \gamma_z \cos\psi\}\cos\hat{\beta} \tag{11}$$

The aerodynamic orientation angles, *viz.* the magnitude of the complex angle of attack and the roll orientation angle, are respectively

$$\hat{\alpha} = \cos^{-1}\frac{\hat{u}}{V}, \quad \hat{\phi} = \tan^{-1}\frac{\hat{v}}{\hat{w}} \tag{12}$$

In the first quadrant, $\acute{\phi}$ is given by

$$\acute{\phi} = \cos^{-1}\left|\frac{\sin\theta\cos\psi}{(1 - \cos^2\theta\cos^2\psi)^{1/2}}\right| \tag{13}$$

with appropriate forms of the $\cos^{-1}$ relationship in the other quadrants. The angle between the complex angle-of-attack plane and the vertical plane through the velocity vector is then $\phi + \acute{\phi}$, so that the angle γ defining the orientation of the lift surfaces with respect to the complex plane is

$$\gamma = \phi + \acute{\phi} \pm n\pi/2 \tag{14}$$

where n is an integer determined by the symmetry of the configuration analyzed. For cruciform symmetry γ is in the range $0 < \gamma < \pi/2$.

Local Aerodynamic Analysis

Angular motion data are analyzed by means of the RL technique[5-7,9,11]. The reconstructed data set is found by superposition of a primary tricyclic solution

$$\xi_1 = K_1 e^{i\Phi_1} + K_2 e^{i\Phi_2} + K_3 e^{i\Phi_3} \tag{15}$$

(K_1, K_2 and K_3 are the tricyclic vectors and Φ_1, Φ_2 and Φ_3 the vector angles) and a series of small-amplitude tricycles obtained by curve-fitting the residuals, so that

$$\xi = \beta + i\alpha = \sum_{j=1}^{n} (\beta_{cj} + i\alpha_{cj}) \qquad (16)$$

where each component is a harmonic or sub-harmonic of the primary motion. The linear solution, Eq. (15), is therefore complemented by a number of free constants to account for the nonlinearities.

In essence, the basis of the technique is that the information content of the complete flight may be used to define the local waveform variations at the peak. Each component in the series is a discrete closed-form equation obtained for the flight as a whole, and when superimposed, the resulting curve has a vastly increased information content at the peak.

The coordinates β, α, X_c obtained from Eq. (16) constitute a very well conditioned data set which may therefore be curve-fitted in short segments at the angular peaks. If the intervals are chosen as short as possible, the effects of variables not represented in the motion equations including variable motion parameters - roll rate, velocity and dynamic pressure - and facility deviations - e.g. flow nonuniformity - will be minimized. Moreover, the aerodynamic coefficients extracted have essentially local values since the angles of attack, sideslip and roll and the velocities do not deviate appreciably from their local values. The pitching moment slope C_{m_α} is thus extracted in terms of the frequency ω at the peak and the pitch damping coefficient $C_{m_q} + C_{m_{\dot\alpha}}$ determined from the difference in shape on the two sides of the peak.

The body axis roll rate p is obtained as a function of distance flown

$$p = p(X) = \dot\phi + \dot\psi \sin\theta \qquad (17)$$

The tricyclic equation is constrained to 8 constants with

$$\xi = K_1 e^{(\lambda_1 + i\omega_1)X_c} + K_2 e^{(\lambda_2 - i\omega_2)X_c} + K_3 e^{i(p_3/V)X_c}$$
$$\omega_1 - \omega_2 = (I_x/I_y)(p_3/V) \qquad (18)$$

where $p_3 = p(X_c)$ is determined at the angular peak. Since the angular acceleration in roll depends primarily on the total angle of attack, the effective local roll rate is defined to be that which is developed at the mean angle of attack for the interval. Using subscripts 1 and 2 to denote the two sides of the peak,

$$p_3 = \{p(X_{c_1})_{\alpha_R = \bar\alpha_m} + p(X_{c_2})_{\alpha_R = \bar\alpha_m}\}/2 \qquad (19)$$

The data obtained from one or from several flights are correlated with the local angle of attack $\bar\alpha$, the roll orientation angle γ (Eq. 14) and with the relative angular excursion

$$E = (\alpha_{pk} - \alpha_{min})/\bar\alpha \qquad (20)$$

where α_{pk} and α_{min} are, respectively, the peak and minimum resultant angles of attack for the segment. The definition of a mean local angle of attack

$$\bar\alpha = \bar\alpha_m = (\alpha_{pk} + \alpha_{min})/2 \qquad (21)$$

was generally used, although several other correlators, including a weighted rms angle of attack of the form

$$\alpha_{wrms} = \left[\frac{1}{x}\int \{(w_x \alpha_R \sin\theta)^2 + (w_\alpha \alpha_R \cos\theta)^2\} dx\right]^{1/2} \qquad (22)$$

where $\theta = \tan^{-1}(d\alpha/dx)$, were also considered.

The local aerodynamic coefficients then have the form

$$C_{m_\alpha} = C_{m_\alpha}(\bar\alpha, \gamma) \qquad (23)$$

$$C_{m_q} + C_{m_{\dot\alpha}} = \bar C_{m_q}(\bar\alpha, \gamma, \omega) \qquad (24)$$

Data Reduction Procedure. The RL technique was implemented in a unified procedure(11). The reconstruction process will proceed automatically while the residuals are correlated, its control being provided by one of several optional starting schemes. The program will automatically recycle the curve-fitting routine with an alternative set of starting conditions when a particular component fails to converge. It has also been organized to resort to an alternative harmonic when the converged solution is physically unacceptable. Then the starting coefficients are the constants of an equation of the form

$$\xi_{2j} = A_j\{K_{11} e^{(d_j\lambda_{11} + ik_j\omega_{11})x} + K_{21} e^{(d_j\lambda_{21} + ik_j\omega_{21})x} + K_{31} e^{i\omega_{3j}x}\} \qquad (25)$$

where A_j, d_j and k_j are multipliers.

The intervals for analysis are selected automatically according to several alternative schemes. For instance, the variation of the aerodynamic coefficients with $\bar\alpha$ around the peak may be determined from analysis over the range of excursions $\Delta_1 \leq E \leq 2 - \Delta_2$ (Δ_1 and $\Delta_2 \ll 2$) where α_{min} is determined in terms of α_{pk}

$$\alpha_{min} = \alpha_{pk}(2 - E)/(2 + E) \qquad (26)$$

The effective, local roll rates are interpolated at each interval, applying Eq. (19).

Investigation of the Technique

A comprehensive study based on analysis of numerically-generated data was undertaken to evaluate the RL technique, while determining the influence of the many flight- and technique-related parameters. The flight characteristics of importance included random noise or data scatter, nonplanar motion, roll rates, nonlinear aerodynamics and vehicle asymmetry, while the technique-related parameters included the number of data

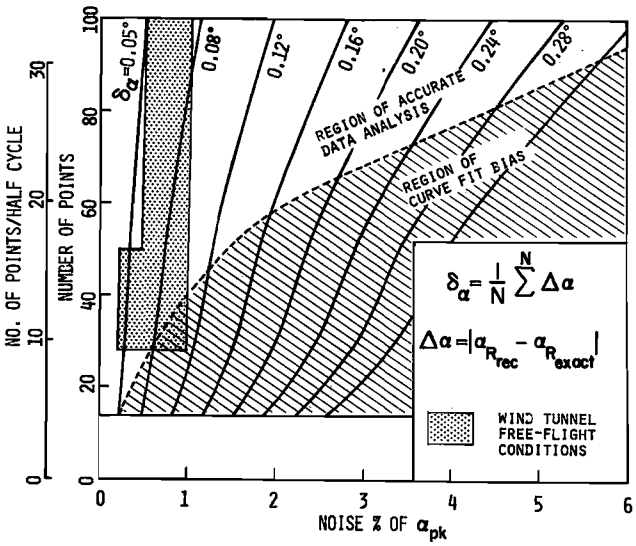

Fig. 6 Requirements on the number of data points

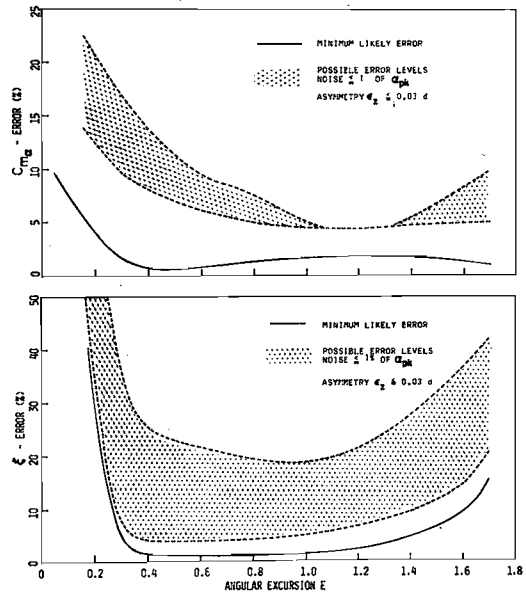

Fig. 7 Error levels in nonlinear derivatives

points, length of interval and flight length, truncation level and the highest harmonics determined. Both representative and extreme values of these parameters were considered in order to determine the limits for application of the technique. A few isolated results are presented here.

Figure 6 presents the number of data points required to maintain mean linear deviations δ_α between the exact and reconstructed motions of 0,05° to 0,32° when the random noise levels are in the range 0 to 6% of α_{pk} (in the test case α_{pk} = 13,5°). The dotted line demarcates conditions for accurate data reconstruction and for biased curve fits. The results are applicable to arbitrary free-flight motions of small eccentricity ($\alpha_{min}/\alpha_{pk} \leq 0,3$), free of systematic errors, and may be used to estimate the number of frames or data stations required to achieve given accuracies when the data acquisition system limitations are known. Corresponding conditions for wind-tunnel free-flight tests are shown for reference in Figure 6.

The optimum flight segment lengths are 1,5 to 1,75 half-wavelengths for noise levels of 0,5% or lower and 1,75 to 2,5 half-waves for noise levels between 0,5% or 1,0% of α_{pk}. The number of harmonics determined is dictated by the number of points and the noise level. The highest harmonics practicable are the 5th and 7th in the cases of $C_{m_q} + C_{m_{\dot\alpha}}$ and C_{m_α}, respectively, and since the shortest interval length is determined by the highest harmonic, the limiting excursions are found to be E = 0,12 and 0,06, respectively. When seeking a specific effect, certain criteria for the quality of the data are immediately implied: For instance, to determine the local waveform variation at E = 0,08, the 6th harmonic must be extracted correctly. The limiting noise level is then 0,5% of the peak angle. Also, 8 and 16 points per half-wave are respectively required to reveal harmonics above the 3rd and 4th.

The probable levels of error in the pitching-moment slope and damping factor ξ extracted from nonoscillatory motion of the missile model, where these coefficients are highly nonlinear, are shown in Figure 7. The minimum error represented that which could result under near-optimal conditions for analysis, where noise levels do not exceed 0,5% of α_{pk} and the model asymmetries are small. On the other hand, the maximum error was representative of the worst conditions which could be expected in the type of free-flight analysis described above; accordingly, nonoptimal conditions were considered, including 1% noise, an unrealistically large mass asymmetry of ε_z = 0,03 d and nonoptimal local roll rates.

Compared with $C_{m_q} + C_{m_{\dot\alpha}}$, C_{m_α} is generally less sensitive to the effective, local roll rates at small E values, and therefore, the maximum error conditions shown in Figure 7 as based on the analysis using Eq. (19) are probably more favourable in the case of the pitching moment slope. An example of these sensitivities is presented in Figure 8 for a bistable model having nonlinear dynamic and static moments and a large mass asymmetry.

It was concluded that the nonlinear variations of both static and dynamic derivatives can be accurately determined under near-optimal conditions representative of wind tunnel free-flight missile tests (0,5% noise, $\varepsilon_z/d < 0,01$) and will be quite well-defined under adverse conditions, for instance, where a specific asymmetry must be simulated ($\varepsilon_z/d \leq 0,03$).

Free-Flight Technique

The problem of achieving flights of significant duration for reasonably large models is fundamental to wind tunnel free-flight testing of lifting vehicles, and, in particular, vehicles in the high manoeuvrability category. The free motions of models of these vehicles are characterized by large, seemingly-erratic lateral displacements which are the concomitants of low pitch frequencies and large roll responses in motion trimmed at significant angles of attack. Such conditions make it difficult to sustain any angular motion and if approached by conventional wind tunnel or ballistic range methods, the models will not remain in sight

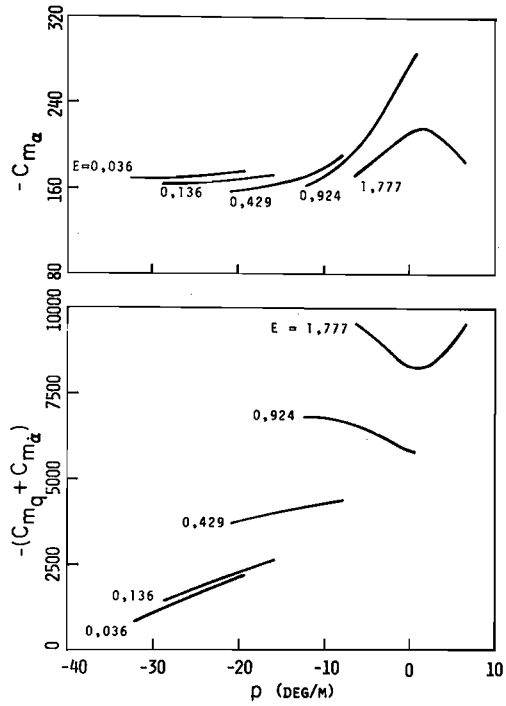

Fig. 8 Sensitivity of derivatives to roll rate

long enough for any useful information to be captured.

Essentially, the difficulties are overcome here by imparting optimal initial conditions at launching, to provide control of the trajectory shape and development of angular motion for maximal utilization of the observation space. Models are launched at zero angle relative to the launch gun and angular acceleration is imparted which causes the maximum angle of attack and the associated swerve to be developed only after the model comes into the field of view.

The principle is implemented in the 'pitch-jet' launching system[8-11] depicted in Figure 9. The launch gun comprises a piston moving within a partially vented cylinder filled with high-pressure nitrogen and two separate forward reservoirs in the gun nose to feed air pressure to the gun head. The piston accelerates uniformly until it approaches the end of its stroke where its energy is dissipated in an air cushion, upon which the model travels forward, guided between a rail and a shroud. An air jet, fed by compressed air within the piston, blows on the model tail after it is free of the rail to initiate a nose-up pitching motion. The equations of motion of the launch gun/pitch jet/model system were integrated to predict its performance as a function of the associated parameters and test conditions[8,11].

A rapid downwards displacement, opposed to the initial swerve direction, is achieved by means of a suitable launch gun depression angle and allows the model wake to become free of interference sooner. This permits the use of release points closer to the observation area, or test rhombus, as shown in Figure 10. The basic differences between launch configurations for stable and bistable models are also apparent from Figure 10 and clearly necessitate large adjustments of the launch gun position and attitude. This is facilitated by an articulated strut which extends through a rectangular slot into the tunnel interior to support the launch gun. The mechanism provides for overall adjustments of -8,5° to 6,5° in gun angle, and 200 mm in both vertical and horizontal location of the release point, while the piston stroke may be adjusted through a range of 60-150 mm. A view of the launch gun and strut with an aircraft model is depicted in Figure 11.

All models have a tendency to roll due to induced rolling moments and tunnel flow non-uniformities and, to a lesser extent, small asymmetries. The incipient departure of the trajectory can be delayed by imposition of suitable combinations of yawing and rolling impulses to fold the trajectory around on itself in corkscrew fashion. Since the overall lateral displacement resulting

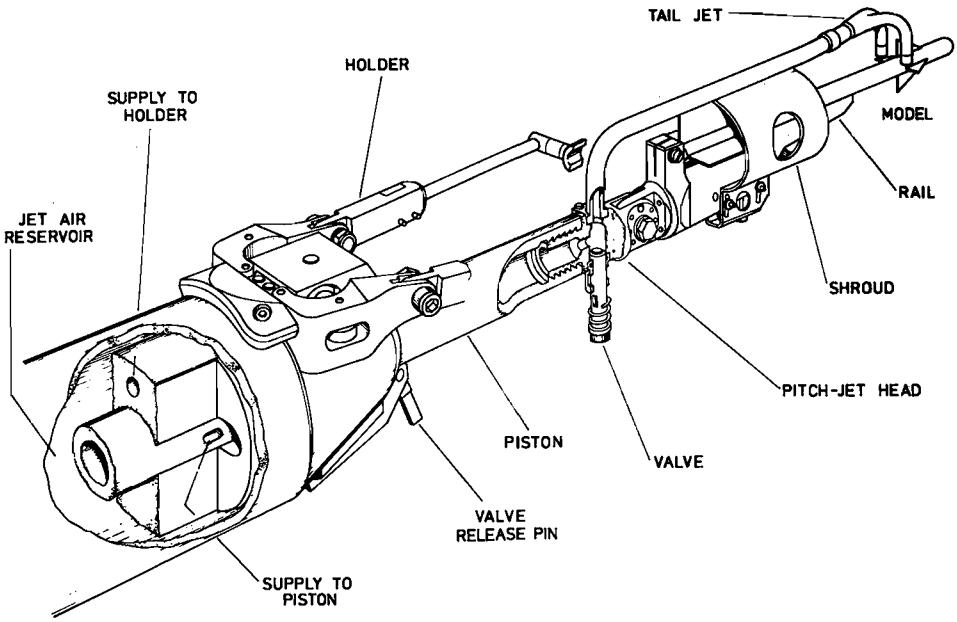

Fig. 9 Pitch-jet launching system

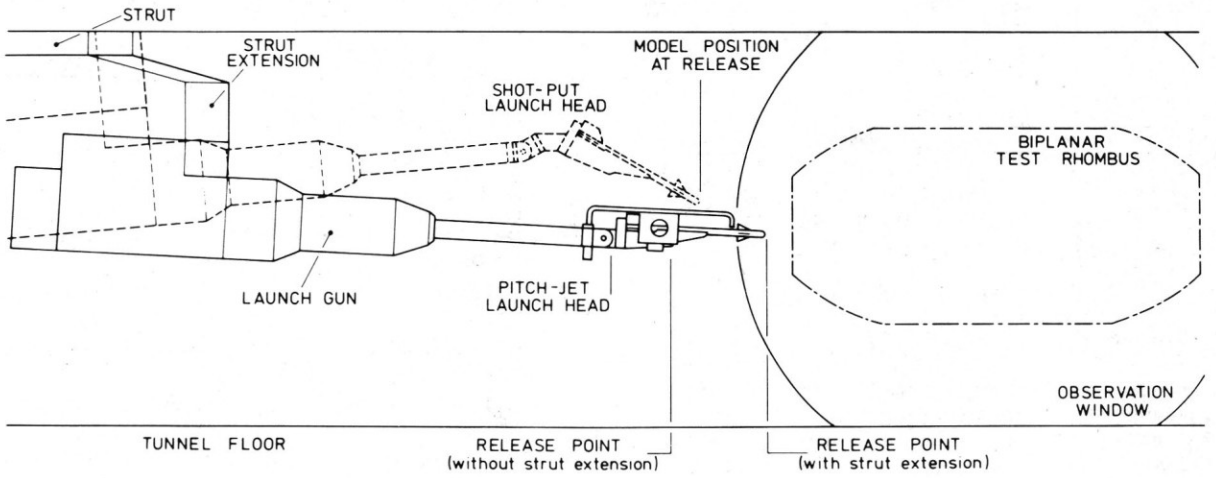

Fig. 10 Launch configurations

from swerve is smallest in nonplanar motion of high eccentricity, this may become a necessary condition when very large swerve amplitudes have to be accommodated.

When the criterion is to generate representative roll rates and to avoid a resonance condition, the model is forced to despin to zero roll rate in the vicinity of the first angular peak. This can be achieved using fin roll tabs and a pitch jet placement to produce opposing roll torques. Some of the arrangements used are shown schematically in Figure 12. Higher roll rates have been achieved on slender models at large angles of attack by means of an optional spin head.

Fig. 11 Aircraft-like model on the launch gun

The question of model design for nonoscillatory flights is quite complex as a large number of parameters relating to the launching geometry, model physical parameters and the test conditions have to be taken into account. Many of the criteria are contradictory so that the optimization of these parameters provides a balance between the requirements for protraction of the flight duration and maximization of the angular responses. The optimum flight may be thought of as having an observation duration equivalent to the optimum segment for data reduction derived in the above analysis, while the angular responses are maximized with respect to this requirement. The key parameter in this trade-off is the model mass and the overall optimization is performed by studying all of the parameters collectively in a trajectory simulation(11).

The requirement of correlating aerodynamic stability data for consistent values of the data reduction parameters was facilitated by the repeatable performance of the complete launching system and by the high degree of manufacturing precision of the free flight models.

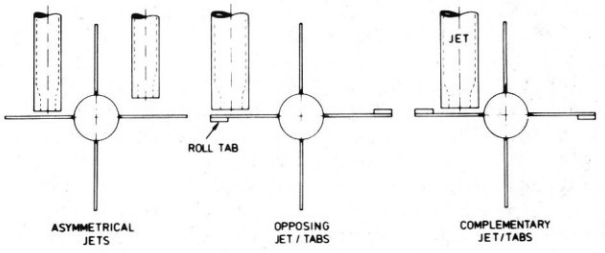

Fig. 12 Jet and trim tab configurations

Free-Flight Tests of an Air-to-Air Missile Configuration

The class of air-to-air missiles typified by the canard missile studied is particularly interesting from a point of view of dynamic stability by virtue of characteristically sensitive aerodynamics, introduced as a consequence of the design objectives of destabilization for increased manoeuvrability. This sensitivity is manifested over the complete angle of attack range from 0 to 25°, as the concomitants of wing-body-tail interference, flow separation and vortex shedding.

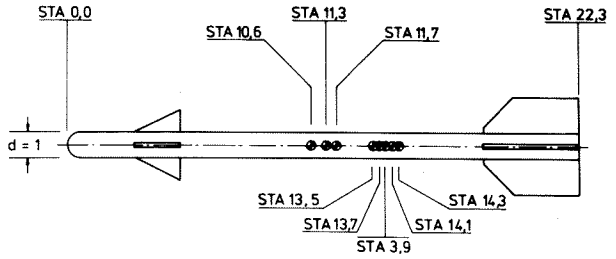

Fig. 13 Test configurations

Test Programme

The test configuration flown in the 0,46 x 0,46-m Blowdown Tunnel consisted of a 22,3 fineness-ratio hemisphere cylinder of diameter 7,25 mm with flat lift surfaces and centre-of-mass locations as far aft as 14,35 diameters d from the nose. The range of mass centres depicted in Figure 13 were defined to yield configurations representative of, and bracketing the stability margins before and after firing of missiles in the class described. A test Mach number of 0,7 was chosen, to be representative of subsonic deployment.

Both stable and unstable motions were investigated, the latter induced for the bistable centre-of-mass locations, i.e. x_{cg} = 13,5 d to 14,3 d. Of the bistable flights, however, only the well-conditioned motions were analyzed in great detail for purposes of correlation. Results of the raw data analysis have been well documented[9,11,12] and are not discussed here; however, brief reference is made to the "P-E signatures" which provided the basis for obtaining the local roll rates. The quantities in Eq.(19) are determined from p/V vs E data. This is represented graphically by plotting p as a function of E, where p is in deg/m. Examples are presented in Figures 14 and 15 for bistable flight with x_{cg} = 13,9 d and 14,35 d, respectively. The depth of the horizontal loops at any value of E is indicative of the roll rate variation at that level for the angular peaks concerned. So, for instance, the first peak in Figure 14 exhibited a small roll response, making it suitable for analysis, while the second was accelerating to resonance.

The reconstructed angular motions of three types of nonoscillatory flight are depicted in Figures 16 to 18. The first is the characteristic small-angle motion having a kink near the trim angle of attack (the aeroballistic angles appear in Figure 16) and the second, a typical large-angle motion in which two peaks could be observed (Figure 17). The reconstructed resultant angle of attack α_R and the actual, transformed experimental data are displayed in Figures 17 and 18. The quality of raw data obtained in this test programme was quite consistent, with noise levels of around 0,5% of α_{pk} and rms deviations from the reconstructed curves of *ca.* 0,08°. Note that the complete flights were somewhat longer than the reconstruction segments shown in these plots.

The differences in time required for the terminal oscillatory motions to cease in the examples of Figures 16 and 17 reflects the different amounts of damping present at the respective amplitudes α_{pk} = 8,5° and 17,8°, (x_{cg} = 13,9 d in both cases). Figure 18 is an example of the

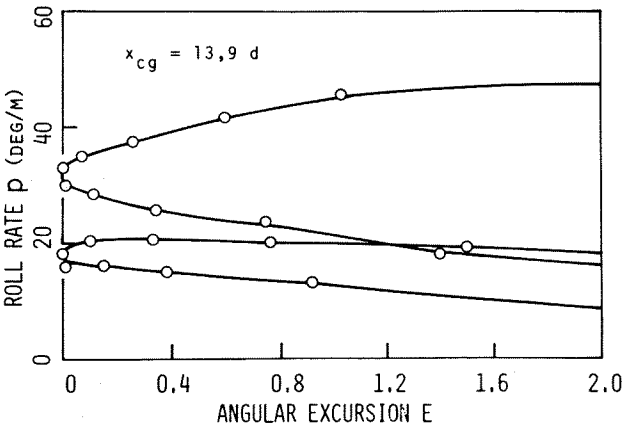

Fig. 14 P-E signature of a terminal oscillation

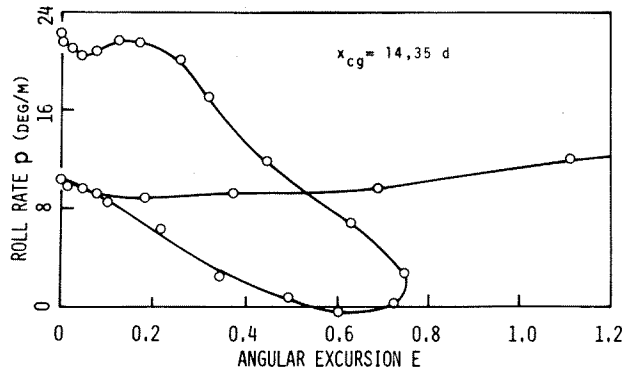

Fig. 15 P-E signature of motion at large trim

reconstructed motions of the most destabilized configuration tested (x_{cg} = 14,35 d). The model is unable to traverse the neutral condition from the peak angle α_{pk} = 13,7° and immediately settles down to a trim angle of near 12°. This model is probably substantially less stable than the most destabilized air-to-air missile, which might trim at an angle of 6°, and is representative of the limiting case for half-cycle nonoscillatory motion in the Blowdown Wind Tunnel on this model scale.

Local Aerodynamic Results

Briefly stated, the prime objective of this programme was to determine the nonlinear dependence of the direct moment derivatives on the local angle of attack and centre-of-mass location, when the frequencies and roll orientation angles are well correlated. A secondary objective was to study various modes of unstable motion to which the missile configuration was susceptible. An effective linear aerodynamic analysis was also performed to obtain certain complementary information, published elsewhere[9,11], including drag coefficients and static and dynamic lift derivatives, required in a trajectory simulation validation[9] of the free-flight experiments.

The local aerodynamic data presented were correlated for consistent values of the various data reduction parameters in order to achieve the quantitative results of the first objective stated above. The flights analyzed in detail had small motion eccentricities, $\alpha_{min}/\alpha_{pk} \leq 0,4$ and non-

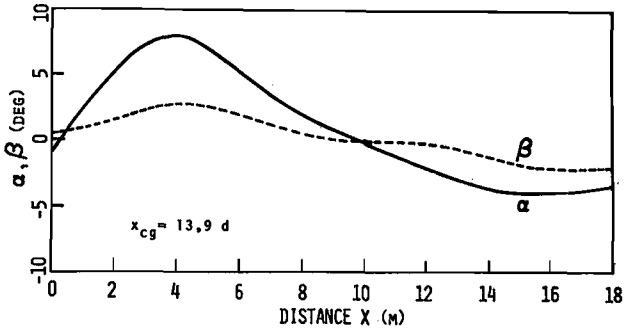

Fig. 16 Small-angle nonoscillatory missile motion

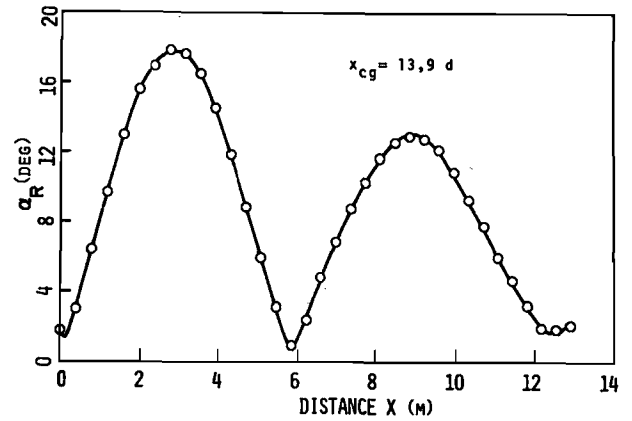

Fig. 17 Large-amplitude terminal oscillation

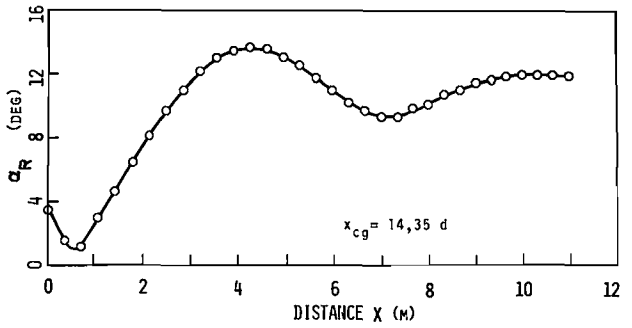

Fig. 18 Extreme, nonoscillatory motion

resonant frequencies $|p/\omega|_{pk} \leq 0{,}5$, while in most cases the rotational frequencies lay in the range $0{,}004 < (\omega d/V)_{pk} < 0{,}006$ and γ_{pk} in the range $15^o < \gamma_{pk} < 20^o$.

The C_{m_α} and $C_{m_q} + C_{m_{\dot\alpha}}$ data for the x_{cg} = 13,9 d configuration are plotted as functions of the local angle of attack in Figures 19 and 20, respectively. The differences in slope of data from individual flights evident in the C_{m_α} plot are attributed partly to effects of truncation in the reconstructions concerned and partly to inconsistent tunnel flow angularity which also contributes to the general scatter. The general correlation could be improved if more flights were available at the same conditions, but the inconsistencies due to flow nonuniformity would be very difficult to eliminate and could only be minimized here - all the tests were run at the same stagnation and supply pressures to ensure that the control valve opening angle would be repeatable. Nevertheless, despite this uncertainty, the results are quite coherent considering the extreme sensitivity of the data.

The characteristic trends visible in Figures 19 and 20 confirm the qualitative interpretation suggested above in the context of Figures 16 and 17: While the bistable missile motion is highly damped at low angles, the dynamic stability coefficient plunges to zero near $\bar\alpha = 13{,}5^o$ before rising to relatively constant, stabilizing values at higher angles of attack. The data of Figure 20 would appear to suggest that a discontinuity in $C_{m_q} + C_{m_{\dot\alpha}}$ exists in the region of $\bar\alpha = 11^o$. The static stability on the other hand, exhibited a trend of decreasing stability at angles of attack above $17{,}5^o$.

The variation of static stability with centre of mass of the canard model is presented in Figure 21. The $\bar\alpha = 0$ results correlate as a straight line which intercepts the horizontal axis at $x_{cg}/d = 13{,}56$, representing the limit case for oscillatory motion; at centres of mass just aft of this position, the motion becomes bistable and the concomitant trim angles grow rapidly with further destabilization: The experimentally-determined trim angles are presented in Figure 22. The data shown in Figure 21 for nonzero values of $\bar\alpha$ were correlated at $\bar\alpha = 12^o$, corresponding to the lowest amplitude at which C_{m_α} could be determined for the most unstable configuration tested. Since the curves are not parallel, a proportionately larger destabilization with decreasing stability margin at higher $\bar\alpha$ is indi-

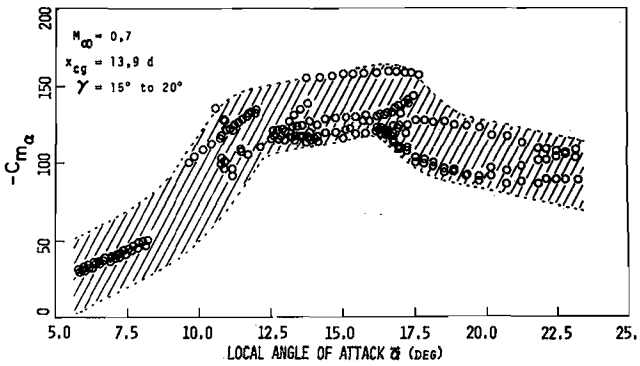

Fig. 19 Local $C_{m_{\dot\alpha}}$ free-flight data

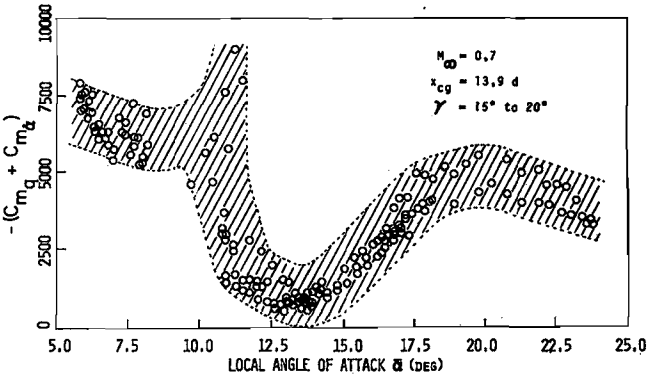

Fig. 20 Local $C_{m_q} + C_{m_{\dot\alpha}}$ free-flight results

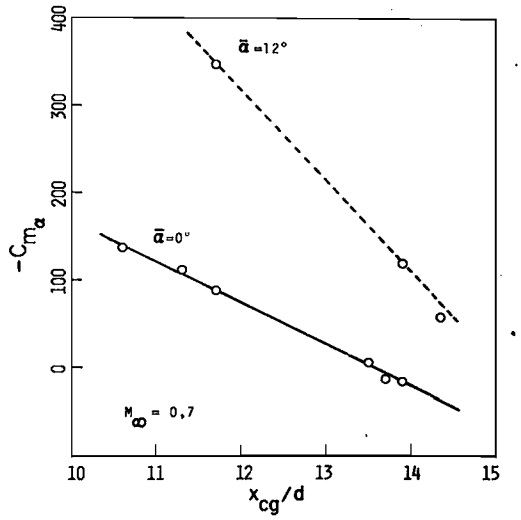

Fig. 21 Local C_{m_α} vs centre-of-mass parameter

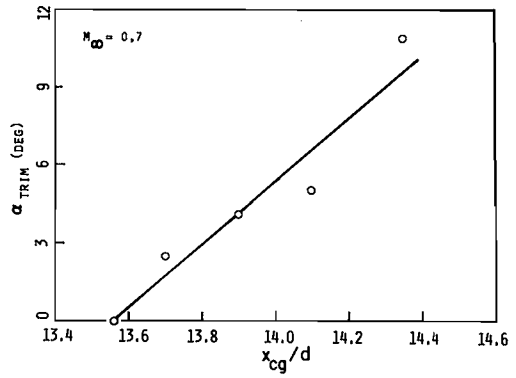

Fig. 22 Bistable trim angles

cated. This implies that C_{m_α} does not transform in a simple manner to unstable centres of mass. Moreover, $C_{m_q} + C_{m_{\dot{\alpha}}}$ is far more difficult to transform between different centres of mass.

The conclusion which must be drawn from this observation is that stable model results cannot be used to predict the stability characteristics of destabilized configurations of the type considered here. Consequently, there does not appear to be an alternative to tests at the actual centres of mass, at least in the case of high-manoeuvrability flight vehicles.

Motion Instabilities

It was hoped that, in the long term, the RL technique could be applied to both of the basic motions of pitch oscillations and coning. In the latter case, the moment derivatives would be correlated with the coning rate ν as required in the force model of Eq. (1), following the formulation of Tobak and Schiff[20]. While quite feasible, this would necessitate some further development of the RL procedure; therefore, in the investigation under discussion the quantitative analysis was limited to pitching and plunging motions of small eccentricity, while more eccentric and near-circular motions were studied in a qualitative sense only.

The destabilized canard missile was found to be prone to instabilities associated with inhibited roll rates in near-circular motion. One such flight is documented in Figure 23 with the angular motion and roll rate referred to the flight co-ordinate system. The motion initially has a moderate eccentricity and a fairly low roll rate, increasing uniformly through the first peak until the nutation frequency is approached in the vicinity of the second peak (X ≈ 8,0 m). The roll rate then locks in at around $-30\bar{\delta}$/m, and is sustained until a divergence of the pitching and yawing motion and a roll acceleration occurs. Instabilities ensuing from roll lock-in appeared to be functions of angle of attack and motion eccentricity, as well as

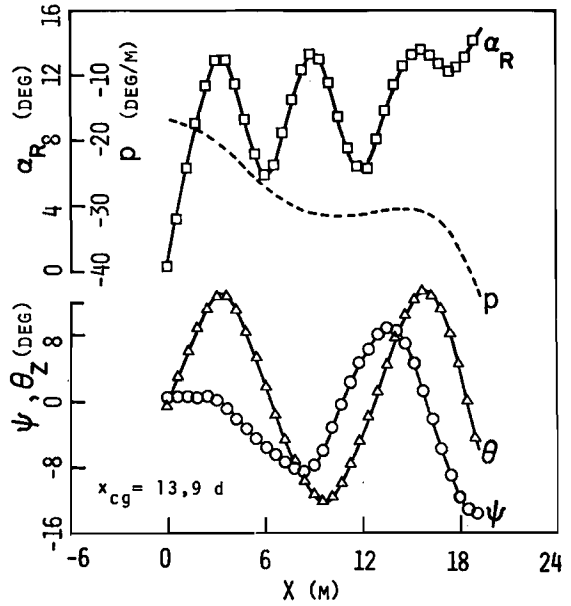

Fig. 23 Divergent, elliptical missile motion

asymmetry. Nondivergent, limit-circular motions were observed when the roll rates were initially lower. Resonating flights of the destabilized model were naturally easy to generate since all that was required was a sufficiently large asymmetry.

Lunar motions occurred in precessions of small eccentricity, such as the large-amplitude flight depicted in Figure 24 (α_{pk} = 24°). The aerodynamic roll angle ϕ and roll orientation γ are shown over the first half-wave. The roll rate varied in phase with the angle of attack but is

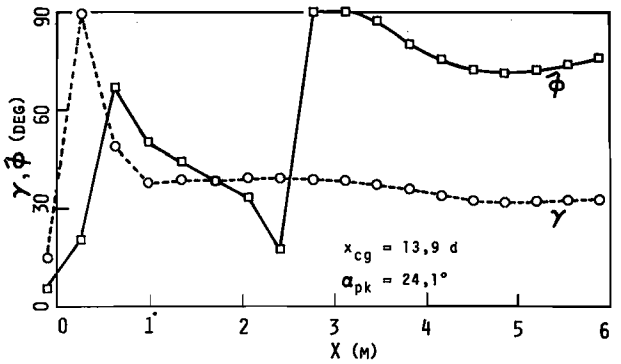

Fig. 24 High angle-of-attack lunar motion

well below resonance at its maximum of -24°/m. γ quickly settled down to a value of approximately 38° while $\dot{\phi}$ locked in at roughly 72°.

In summary, it may be observed that, as a result of nonlinearities and aerodynamic cross-coupling, the motion eccentricity in flight of the canard missile will tend to increase. In large-angle, lunar motion at low roll rates the resulting motion could be a stable limit circle; on the other hand, if roll lock-in occurs, the roll rate will speed up as the eccentricity increases and the coning motion will diverge.

Since the control characteristics of the canard missile are determined, *inter alia*, by aerodynamic inputs, a potential free-flight instability coupled with a loss in dynamic damping could produce twitchy responses and loss in manoeuvrability, particularly in the medium angle-of-attack range ($11° < \bar{\alpha} < 17°$) (see Figure 20). It is rather disconcerting to note that the observed instabilities all tend to occur in the circular condition, while the primary mode of a guided missile employing a twist-and-steer control system, is precisely that of circular, coning motion.

Aircraft Model Free-Flight Analysis

Whereas the desirability of complementing aircraft dynamic testing procedures with free-flight tests under laboratory conditions has long been recognized, the feasibility of the latter was questionable and all but ruled out. Consequently, little progress was made until recently, when, after it had been proposed that an aircraft-like model tested at the National Aeronautical Establishment[13-15] also be studied in free-flight, an analysis was performed to demonstrate the feasibility of such tests.

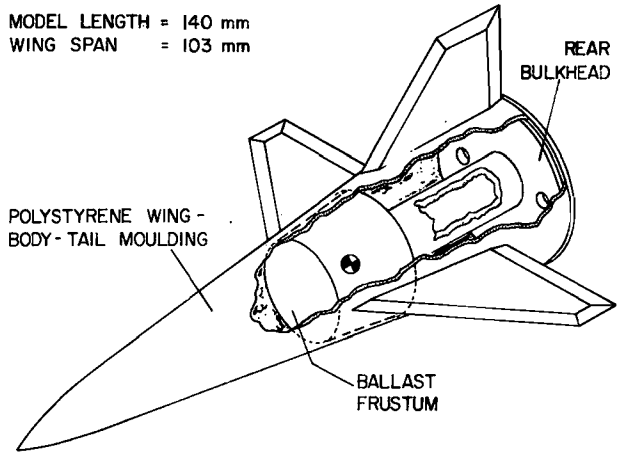

Fig. 25 Aircraft-like free-flight model

Preparations for Aircraft-Model Tests

At the same time, a half-scale free-flight replica of the NAE aircraft-like configuration was designed for tests in the 0,46 x 0,46 m Blowdown Tunnel. The model layout illustrated in Figure 25 was designed by means of a computer program[21,11] for a centre of mass, x_{cg} = 0,68 d, located at the moment reference centre used by Orlik-Rückemann et al[13,14]. Following the procedure outlined above, the model mass distribution was optimized by simultaneously maximizing the angular responses and minimizing the swerve on the basis of 6 DOF simulations.

Suitable launching hardware was manufactured for tests involving aircraft models (see Figure 11) and preparations were made for utilization of the mono-planar, optical data acquisition concept introduced above (Eqs. (3) to (8)).

6 DOF Trajectory Simulations

A 6 DOF, rigid-aircraft trajectory program incorporating aerodynamic cross-coupling and arbitrary asymmetries was used in this study. All of the static and dynamic coefficients were accessed through 2-dimensional table look-up and quadratic interpolation, in the interests of preserving the experimentally-determined nonlinearities.

Several flights of the aircraft model were simulated using available aerodynamic coefficients at Mach 0,7 and initial conditions representative of the pitch-jet launching system operating range. Except for the centres of mass, which were displaced by Δx_{cg} = -0,01 d and -0,02 d from the nominal reference x_{cg} = 0,68 d, the measured model parameters were used throughout.

High Angle-of-Attack Motion. Since the available high-angle static data[13] were functions of α only, these numerical simulations had to be constrained to planar motion. The vertical-plane motions and pitch angle histories of two flights with maximum angles α_{pk} = 40° are presented in Figure 26. This shows that one-wavelength, nonoscillatory motions are possible at high amplitudes with the small increases in static margin, although the model is statically unstable over much of the α-range at x_{cg} = 0,68 d. The swerve displacements for the Δx_{cg} = -0,01 d and -0,02 d motions were 0,22 m and 0,13 m, respectively, which may easily be confined within the observation space.

Medium Angle-of-Attack Motion. General nonplanar motions were generated for angles of attack up to 17°, corresponding to the range of the available static coefficients (the dynamic derivatives[14] were available for angles up to 41°). Angular motion histories for the two mass centres are

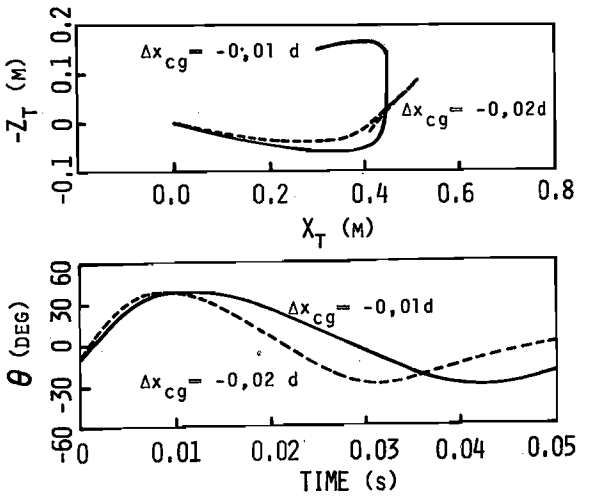

Fig. 26 High-α aircraft model motion (α_{pk} = 40°)

plotted in Figures 27 and 28 for the same initial conditions. The Δx_{cg} = -0,01 d model configuration could not achieve a peak angle in the range $12^o < \alpha_R < 21^o$ by virtue of the nonlinear stability characteristics. The Δx_{cg} = -0,02 d configuration, on the other hand, displayed the generic nonoscillatory motion encountered in flights of the canard missile (Figures 2 or 16).

The nonlinear rolling moment C_ℓ has a significant effect on the lateral displacement. The transverse-plane motions of the Δx_{cg} = -0,02 d flight having a nonzero rolling moment is compared in Figure 29 with its counterpart for C_ℓ = 0. While this effect could not be investigated in detail for lack of nonlinear C_ℓ data, it is unlikely that the actual swerve amplitudes would significantly exceed the maximum simulated. It should also be noted that the facility of mechanically inhibiting the rolling, nonplanar motion to limit the overall displacements was not represented in the simulations.

The maximum lateral displacements to be contended with are therefore in the vicinity of 0,4 m, for motions at angles of attack up to 40°. Thus, through extension of the existing free-flight technology, the aircraft model could be successfully flown at Mach 0,7 in the Blowdown Tunnel, provided that its stability margin is increased by Δx_{cg} =-0,01 d at high angles, and -0,02 d at medium angles, and that the full test section is available for observation. While use of the existing biplanar system could be feasible if the model should be further stabilized, it is considered eminently more desirable to utilize the proposed monoplanar approach in order to preserve the neutral or marginal stability characteristic.

Wind Tunnel Flow Nonuniformity

Unfortunately, any approach based on utilization of the full test section imposes particularly stringent criteria for tunnel flow conformity. This problem was considered in some detail and in order to explore the limitations on free-flight data reduction, a mathematical model of the empty-tunnel flow distribution was developed to facilitate an analysis based on very limited flow angularity calibration data. The ultimate objective would be to evaluate the sensitivity of the aerodynamic derivatives to flow angularities.

While this investigation has yet to be taken to a definitive conclusion, it has been tentatively observed that flow angularities of amplitudes in excess of 0,2° could impair the ability to extract dynamic cross-coupling derivatives, while the direct derivatives could probably be determined satisfactorily in the presence of angularities of the order of 0,5° under otherwise favourable conditions.

Motion Analysis

The following is suggested here as a possible approach for the data reduction: the RL method will be used to obtain the direct derivatives as functions of $\bar{\alpha}$ and γ. These data will be used to model a numerical-integration data reduction procedure[22] and fitted to the motion data using initial conditions determined from the local analysis of the flight. The dynamic cross-coupling

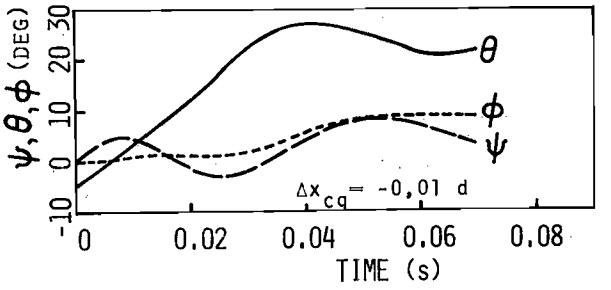

Fig. 27 Nonoscillatory motion at medium angles

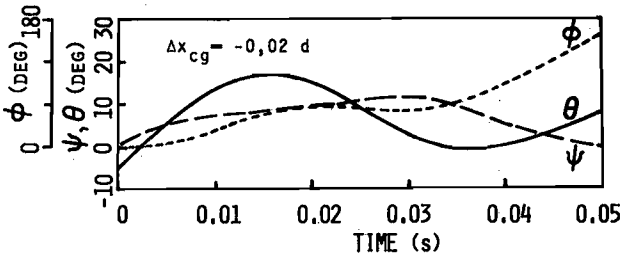

Fig. 28 Rolling, oscillatory aircraft model motion

may, in principle, be represented in the differential equations although this would greatly increase the complexity of the data reduction.

Since the magnitude of random data acquisition errors which can be tolerated in nonplanar motion is now well understood and can be limited to rms levels of between 0,06° and 0,20°, the success of the method proposed would be determined primarily by the extent to which the superimposed effects of the cross-coupling moments are clouded by systematic deviations due to flow nonuniformity.

Either way, it would be possible to correlate the captive model results with the free-flight data even before comprehensive data reduction is undertaken, using an indirect method: The observed wind-tunnel trajectories may be simulated for the most complete set of dynamic derivatives available, where the initial motion conditions could again be derived from local analysis. Should the computed

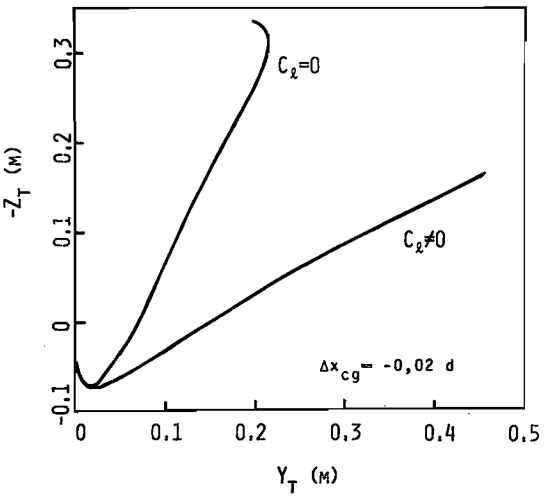

Fig. 29 Transverse-plane motions

trajectories closely match the observed flights, this would at once provide much confidence in the captive model dynamic data and verify the force model used. This is precisely the first step in the validation procedure described with reference to Figure 1.

Conclusion

The rationale underlying the utilization of data gathered in captive- and free-model dynamic stability tests of high-performance aircraft and missiles was examined in the context of the design objectives of high manoeuvrability and good flying qualities. It is concluded that free-model tests and, in particular, wind tunnel free-flight tests can fulfil a vital link in the validation of mathematical force models used in simulations of aircraft motion.

Free-flight testing may also be used in a quite direct fashion to extract aerodynamic derivatives of destabilized, high-manoeuvrability vehicles. Following the approach presented for the analysis of nonoscillatory free-flight motion, the aerodynamic nonlinearities could be determined directly and without need for any *a priori* modelling of these nonlinearities in the equations of motion. The capabilities and limitations of the new techniques were explored in depth, leading to certain fairly universal conclusions for the analysis of free-flight motion.

The direct dynamic derivatives of an air-to-air missile configuration were determined, revealing highly nonlinear variations of C_{m_α} and $C_{m_q} + C_{m_{\dot\alpha}}$ with local angle of attack. The dynamic stability data presented were obtained from analysis of instantaneous measurements in free flight, and therefore, in the absence of any physical intrusion into the flow near the model. Such flights are, therefore, the true analogue of the missile motion at that scale, and applicable to full-scale flight provided that sufficient dynamic data are available at both model- and full-scales to define the scale effects present.

Hence, it must be concluded that the destabilized canard missile possesses a real dynamic destabilization characteristic manifested in the medium angle-of-attack range and that the static stability decreases towards higher angles of attack. Moreover, the free-flight motions were found to be basically unstable in the circular mode, with tendencies to roll lock-in and increasing eccentricity in nonplanar motion. The capabilities of the experimental technique extended beyond the swerving capability of destabilized air-to-air missiles: In the course of the test programme, missile models could be flown at trim angles as high as 12^o, where the model centres of mass were probably substantially further aft than their full-scale counterparts.

The feasibility of aircraft model free-flight tests at high angles of attack ($\alpha_{pk} = 40^o$) was discussed on the basis of 6 DOF trajectory simulations of a free-flight model of the NAE aircraft-like configuration. It is concluded that the pertinent direct dynamic derivatives could be determined without difficulty, while the extraction of cross-coupling derivatives would perhaps be limited only by flow nonuniformities. Although the analysis was restricted to the NAE model, the conclusions are equally applicable to arbitrary high-performance aircraft configurations for models of the same wingspan.

A trajectory simulation validation scheme for the corroboration of captive-model, dynamic stability data with free-flight results of an aircraft configuration was proposed. It is considered important that such inter-technique correlations be undertaken in the future. In summary, it may be concluded that the usefulness of the free-flight dynamic testing approach is not only contingent on the ability to extract dynamic derivatives directly, but also lies in the broader objective of aerodynamic data/model validation, with particular advantages for the analysis of high-manoeuvrability flight vehicles.

References

1. Dayman, B., Jr. , "Free-Flight Testing in High-Speed Wind Tunnels", AGARDograph 113, May 1966.
2. Jaffe, P., "Nonplanar Tests Using the Wind-Tunnel Free-Flight Technique", J. Spacecraft and Rockets, Vol. 10, July 1973, pp. 435-442.
3. Holmes, J.E. and Woehr, F.A., "Wind-Tunnel Free-Flight Testing of Configurations with High-Fineness Ratio Bodies", AIAA Paper 71-278. Albuquerque, Mar. 1971.
4. Jaffe, P., "A Free-Flight Investigation of Transonic Sting Interference", JPL TM 33-704, Pasadena, Jan. 1975.
5. Beyers, M.E., "A New Technique for the Analysis of Non-Linear Free-Flight Motion", AIAA Paper 74-614, Bethesda, July 1974.
6. Beyers, M.E., "Identification of Non-Linear Components of Free-Flight Motion", AIAA Mechanics and Control of Flight Conference, AFM Workshop, Anaheim, Aug. 1974 (also, CSIR Report ME 1334).
7. Beyers, M.E., "Technique for Smoothing Free-Flight Oscillation Data", J. Spacecraft and Rockets, Vol. 12, May 1975, pp. 318-319.
8. Beyers, M.E., "Free-Flight Testing of High-Maneuverability Missile Configurations", CSIR Report ME 1453, Pretoria, Mar. 1976 .
9. Beyers, M.E., "Free-Flight Investigation of High-Maneuverability Missile Dynamics", J. Spacecraft and Rockets, Vol. 14, Apr. 1977, pp. 224-230.
10. Beyers, M.E., "Developments in Wind Tunnel Free-Flight Testing", The South African Mechanical Engineer, Sept. 1977.
11. Beyers, M.E., "Analysis of High-Manoeuvrability Vehicles in Free Flight", PhD Thesis, Faculty of Engineering, University of the Witwatersrand, Johannesburg, Dec. 1977.
12. Beyers, M.E., "Rolling Motion of Canard Missiles in Wind Tunnel Free-Flight Tests", CSIR Report ME 1561, Pretoria, Mar. 1978.

13. Orlik-Rückemann, K.J., LaBerge, J.G. and Hanff, E.S., "Static and Dynamic Cross-Derivatives on a Wing-Body-Fin Configuration at Mach 0.7 in NAE 30" x 16" Wind Tunnel", NRC NAE LTR-UA-26, Oct. 1974.

14. Orlik-Rückemann, K.J., Hanff, E.S. and Laberge, J.G., "Direct- and Cross-Coupling Subsonic Moment Derivatives due to Oscillatory Pitching and Yawing of an Aircraft-Like Model at Angles of Attack up to 40^{o} in Ames' 6' x 6' Wind Tunnel", NRC-NAE LTR-UA-38, Nov. 1976.

15. Orlik-Rückemann,K.J., "Aerodynamic Coupling Between Lateral and Longitudinal Degrees of Freedom", AIAA Journal, Vol. 15, Dec. 1977, pp. 1792-1799.

16. Hanff, E.S. and Orlik-Rückemann, K.J., "Wind Tunnel Measurement of Dynamic Cross-Coupling Derivatives", J. Aircraft, Vol. 15, Jan. 1978, pp. 40-46.

17. Ericsson, L.E. and Reding, J.P., "Reynolds Number Criticality in Dynamic Tests", AIAA Paper 78-166, Huntsville, Jan. 1978.

18. Reding, J.P. and Ericsson, L.E., "Dynamic Support Interference", J. Spacecraft and Rockets, Vol. 1, July 1972, pp. 547-553.

19. Ericsson, L.E., "Effect of Sting Plunging on Measured Nonlinear Pitch Damping", AIAA Paper 78-832, San Diego, Apr. 1978.

20. Tobak, M. and Schiff, L.B., "On the Formulation of the Aerodynamic Characteristics in Aircraft Dynamics", NASA TR R-465, Jan. 1976.

21. Beyers, M.E., "Computerized Model Design for Optimum Wind Tunnel Free-Flight Tests", CSIR Report ME 1165, Pretoria, Nov. 1972.

22. Whyte, R.H., Winchenbach, G.L. and Hathaway, W.H., "Analysis of Free Flight Trajectory Data for a Complex Asymmetric Missile Configuration at Subsonic Mach Numbers ", AIAA Paper No. 79-1689, Boulder, Aug. 1977.